Orientational relaxation dynamics in aqueous ionic solution: Polarization-selective two-dimensional infrared study of angular jump-exchange dynamics in aqueous 6M $NaClO_4$

Minbiao Ji[1,2] and Kelly J. Gaffney[1,a)]
[1]*PULSE Institute, SLAC National Accelerator Laboratory, Stanford University, Stanford, California 94305, USA*
[2]*Department of Physics, Stanford University, Stanford, California 94305, USA*

(Received 9 October 2010; accepted 4 December 2010; published online 25 January 2011)

The dynamics of hydrogen bond (H-bond) formation and dissociation depend intimately on the dynamics of water rotation. We have used polarization resolved ultrafast two-dimensional infrared (2DIR) spectroscopy to investigate the rotational dynamics of deuterated hydroxyl groups (OD) in a solution of 6M $NaClO_4$ dissolved in isotopically mixed water. Aqueous 6M $NaClO_4$ has two peaks in the OD stretching region, one associated with hydroxyl groups that donate a H-bond to another water molecule (OD_W) and one associated with hydroxyl groups that donate a H-bond to a perchlorate anion (OD_P). Two-dimensional IR spectroscopy temporally resolves the equilibrium inter conversion of these spectrally distinct H-bond configurations, while polarization-selective 2DIR allows us to access the orientational motions associated with this chemical exchange. We have developed a general jump-exchange kinetic theory to model angular jumps associated with chemical exchange events. We use this to model polarization-selective 2DIR spectra and pump-probe anisotropy measurements. We determine the H-bond exchange induced jump angle to be $49 \pm 5^\circ$ and the H-bond exchange rate to be 6 ± 1 ps. Additionally, the separation of the 2DIR signal into contributions that have or have not undergone H-bond exchange allows us to directly determine the orientational dynamics of the OD_W and the OD_P configurations without contributions from the exchanged population. This proves to be important because the orientational relaxation dynamics of the populations that have undergone a H-bond exchange differ significantly from the populations that remain in one H-bond configuration. We have determined the slow orientational relaxation time constant to be 6.0 ± 1 ps for the OD_W configuration and 8.3 ± 1 ps for the OD_P configuration. We conclude from these measurements that the orientational dynamics of hydroxyl groups in distinct H-bond configurations do differ, but not significantly. © *2011 American Institute of Physics*. [doi:10.1063/1.3530783]

I. INTRODUCTION

The orientational motion of water molecules in general, and hydroxyl groups in specific, affects many solution phase chemical processes including proton transfer and protein activity.[1–3] These hydroxyl group orientational motions occur with three distinct time scales: (1) the diffusive motion of the intact OH···O hydrogen bond (H-bond) on the several picosecond timescale, (2) the 50 fs period librational motion centered along the OH···O H-bond axis, (3) and most importantly, the infrequent but prompt jump reorientation when the hydroxyl group switches H-bond acceptors.[4–7] This dissociation and reformation of H-bonds represents the key dynamical event in water and the H-bond jump exchange mechanism for H-bond switching demonstrates the strong correlation between the H-bond switching and rotational dynamics.[4,6,7]

This general correlation of H-bond and rotational dynamics in water also applies to aqueous ionic solutions.[8,9] In these solutions both water molecules and the anions function as H-bond acceptors, generating water–water H-bond configurations (OD_W), water-anion H-bond configurations (OD_P), and leading to H-bond exchange between these distinct configurations, Fig. 1(a). OD_W and OD_P correspond to hydroxyl group configurations, not molecular configurations, and place no constraints on the other H-bond interactions of the partially deuterated water molecule. These definitions reflect the information content of the measurement, where the deuterated hydroxyl stretch frequency provides direct information about the nature of the H-bond being donated by the excited hydroxyl group. The interconversion of water–water and water–anion H-bonds provides the opportunity to investigate the angular dependence of H-bond switching between these distinct configurations with polarization-selective two-dimensional IR (2DIR) spectroscopy. We have used polarization-selective 2DIR spectroscopy to study H-bond exchange and hydroxyl group reorientation in a solution of 6M $NaClO_4$ dissolved in isotopically mixed water. Two-dimensional IR spectroscopy provides a unique tool for studying equilibrium chemical exchange on the picosecond time scale of molecular species or conformations with distinct vibrational absorption frequencies.[10–14] We utilize a high concentration of $NaClO_4$ to generate an appreciable number of water–perchlorate hydrogen bonds in solution, as reflected by the OD_P absorption in Fig. 1. While the vibrational spectrum of the OD_W

a)Author to whom correspondence should be addressed. Electronic mail: kgaffney@slac.stanford.edu.

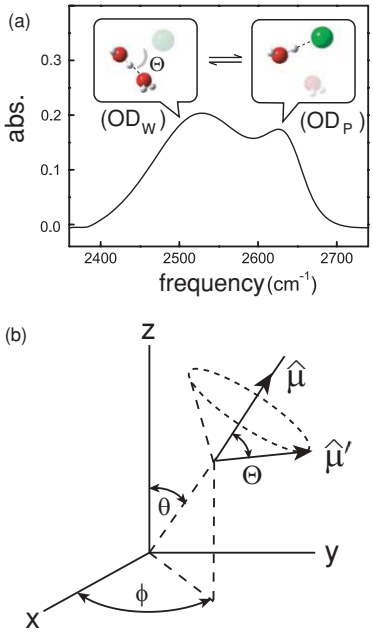

FIG. 1. (a) FTIR absorption spectrum for 6M $NaClO_4$ dissolved in H_2O containing 5% HOD. The lower frequency peak at 2534 cm^{-1} corresponds to the OD groups donating H-bonds to other water molecules (OD_W) and the peak at 2633 cm^{-1} corresponds to OD groups donating H-bonds to a perchlorate ion (OD_P). (b) Schematic of the angular jump in the laboratory frame of reference (x, y, z).

configuration does not differ significantly from isotopically mixed water, we have roughly one ion for every five water molecules, so all local configurations should be very distinct from ion-free water. In addition to the direct influence of the anion on the hydroxyl stretch frequency and dynamics, the influence of the Na^+ cation should not be disregarded. Molecular dynamics simulations give longer residence times for water molecules in the first solvation shell of Na^+, than low charge density anions like perchlorate. The water–cation interaction will restrict the water molecule motion, but if this primarily restricts translational motion and does not significantly disturb the H-bonds being donated by the water molecule it may only subtly influence the dynamics of the hydroxyl stretch.[15]

In this paper we summarize the experimental observation of the large, prompt angle jump associated with H-bond exchange,[9] extract the intraconfigurational orientational dynamics of the OD_W and OD_P H-bond conformations, and present a detailed description of the theoretical model utilized to extract the jump angle from the polarization-selective 2DIR measurements. Our investigation of H-bond exchange relies on previous developments in the theoretical description of rotational dynamics in H-bonded solutions, as well as theoretical models of 2DIR spectroscopy.[16–18] Theoretical models for rotational dynamics originating from librational, diffusive, and angular jump motions have been developed and applied to experimental studies of rotational dynamics in water and aqueous solutions.[19–27] For the diffusive motion of hydroxyl groups with an intact H-bond, models based on diffusive molecular rotors have been used.[28–30] These models result in single exponential relaxation of the hydroxyl group anisotropy with a time constant directly related to the orientational diffusion constant. For hydroxyl group librational motion, the wobbling in a cone model has been used to explain the deviation of the experimental anisotropy from 0.4 near time zero in ultrafast polarization resolved vibrational spectroscopy studies of the hydroxyl stretch in water.[5,31,32] For the jump reorientation, more complicated models have been developed, such as Ivanov's rotational Brownian model,[33] Berne and Pecora's extended diffusion model,[30] and more recently the work of Laage and Hynes.[6,8]

The analysis of our experimental results requires the simulation of polarization resolved 2DIR measurements. Various methods have been proposed to calculate and simulate 2DIR spectra. Molecular dynamics based calculations[4] provide very useful insight into the connection between the mechanism of molecular dynamics and simulated 2D spectra,[4,34] but they do not provide a convenient starting point for experimental data analysis. The two-species exchange kinetic model developed by Kwak *et al.*[16] has been used to successfully analyze 2DIR exchange spectra when the chemical exchange and orientational dynamics can be treated independently. More specifically, the model only accounts for the diffusive reorientation of molecules and assumes that the conformational exchange does not change the orientation of the vibrational transition dipole moment (no angular jump). For coupled vibrational transition dipole moments with arbitrary relative angles, Golonzka *et al.*[35] have developed a theoretical description of polarization resolved 2DIR spectra capable of extracting the angle between the two transition dipoles, but the quasistatic coupling used in the model cannot be applied to chemical exchange. H-bond exchange entangles the conformational and orientational dynamics of water hydroxyl groups and requires the modification of the existing methods for modeling 2DIR spectra. We have developed a self-consistent kinetic model to analyze the jump-exchange dynamics from polarization-selective 2DIR spectra. This model accounts for all three mechanisms for molecule reorientation and allows us to consistently analyze both the 2DIR and pump-probe data with a single set of parameters, thus providing a more reliable procedure for analyzing experimental spectroscopic data.

The separation of the 2DIR signal into contributions that have or have not undergone H-bond exchange also allows us to directly determine the orientational dynamics of the OD_W and the OD_P configurations without contributions from the exchanged population. This proves to be important because the angular jumps associated with H-bond exchange result in orientational relaxation dynamics for the populations that have switched H-bond configurations clearly distinct from the populations that remain in a single H-bond configuration. The simultaneous analysis of the polarization-selective pump-probe and 2DIR spectra within a single self-consistent model for the population and angular dynamics allows for the robust extraction of the orientational relaxation dynamics of the OD_W and OD_P configurations. We have determined the slow orientational relaxation time constant to be 6.0 ± 1 ps for the OD_W configuration and 8.3 ± 1 ps for the OD_P configuration. These time constants exceed the values we extracted previously from a pump-probe anisotropy

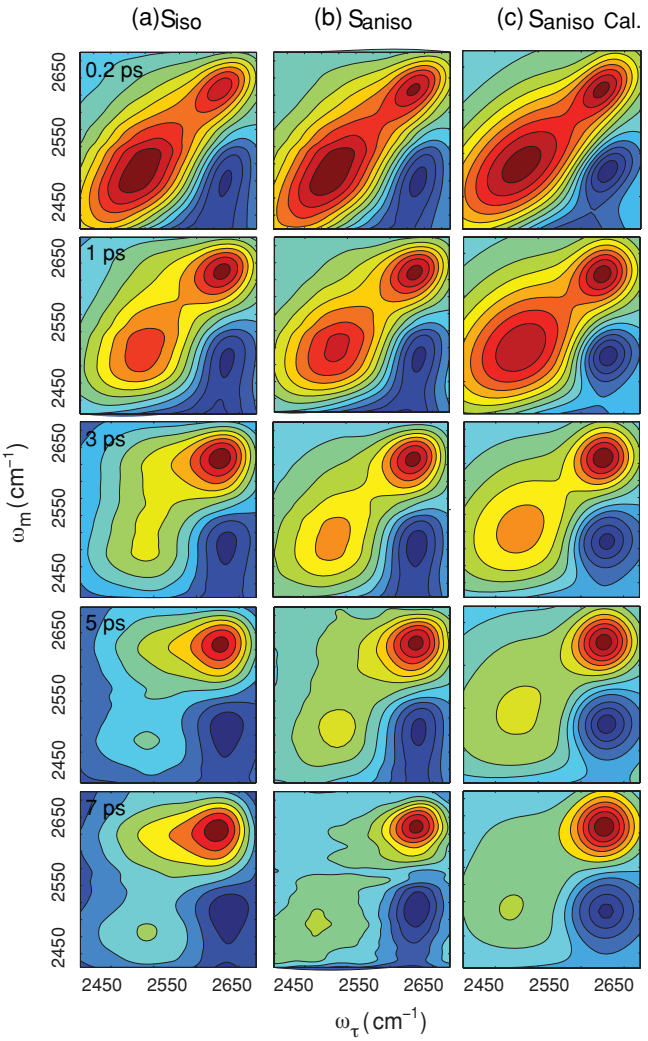

FIG. 2. The experimental isotropic 2DIR spectra $S_{\rm iso}$ are shown in the first row (a), the experiment anisotropic 2DIR spectra $S_{\rm aniso}$ are shown in the second row (b), and the calculated spectra using the response function and the JEK model fitting results are shown in the third row (c).

measurement where we had implicitly assumed that H-bond configuration exchange did not influence the hydroxyl group orientational dynamics.[36] These modified numerical values for the rotational time constants still support the conclusion that the average rotational dynamics of hydroxyl groups in aqueous 6M $NaClO_4$ differ significantly from those of water, independent of the hydroxyl group H-bond configuration.

II. EXPERIMENTAL METHODS AND RESULTS

The dissolution of 6M $NaClO_4$ in isotopically mixed water (5% HOD in H_2O) generates two deuterated hydroxyl stretch (OD) frequencies: OD groups donating a H-bond to OD_W absorb at $\omega_W = 2534\,cm^{-1}$, whereas OD groups donating a H-bond to a perchlorate anion (OD_P) absorb at $\omega_P = 2633\,cm^{-1}$ [Fig. 1(a)]. This spectroscopic distinction between the OD_W and OD_P provides the opportunity to track H-bond exchange dynamics by monitoring the growth in the cross peak intensity in the time-dependent 2DIR spectra.[36,37]

Ultrafast 2DIR spectroscopy monitors equilibrium H-bond switching dynamics on the picosecond time scale,[10,26,29,30,33] by labeling molecules through resonant excitation of the deuterated hydroxyl stretch of isotopically mixed water, and then correlating these initial frequencies ω_τ with the final stretch frequencies ω_m associated with these same excited molecules after an experimentally controlled waiting time T_w. In a 2D spectrum, the cross peaks only reflect H-bond exchange events in which the hydroxyl group switches between the OD_W and OD_P configurations. We have added polarization selectivity to the 2DIR spectroscopy measurement in order to access the orientational dynamics associated with H-bond exchange.[9] Two-dimensional IR experiments with various polarization controls have successfully investigated the interaction and relative orientations of anharmonically coupled vibrations,[17,35] and enhanced the relative intensity of cross and diagonal peaks resulting from anharmonically coupled vibrations.[38,39]

We heterodyne detect a three pulse stimulated photon echo signal to generate our polarization-selective 2DIR spectra. For our polarization-selective 2DIR spectroscopy, the first two pulses controlling the frequency labeling of OD stretches always have the same polarization and preferentially excite transition dipole moments parallel to the excitation polarization. The third pulse, the echo signal, and the local oscillator have the same polarization, which is set either parallel or perpendicular to the polarization of the first two pulses. During the T_W waiting time, the excited molecules randomize their orientation within the OD_W and OD_P configurations, and undergo H-bond exchange between the OD_W and OD_P configurations. If the H-bond exchange minimally perturbs the vibrationally excited hydroxyl group orientation, both the diagonal and the cross peak intensities will exhibit similar polarization dependence. However, if the molecules exchange via large angular jumps, the cross peak signal that results solely from OD_W–OD_P exchanged populations will show distinctly different polarization dependence from that of the diagonal peaks, as will be discussed in Sec. III.

Experimental 2D spectra with parallel (S_{zzzz}) and perpendicular (S_{zzyy}) polarization geometries can be found in our previous work.[9] We show the isotropic ($S_{\rm iso} = S_{zzzz} + 2S_{zzyy}$) and anisotropic ($S_{\rm aniso} = S_{zzzz} - S_{zzyy}$) spectra in Figs. 2(a) and 2(b), respectively. While the isotropic spectra show a clear growth in the cross peak intensity with increasing T_W, indicating the occurrence of H-bond exchange, the anisotropic spectra have vanishingly small cross peak intensities. The very weak polarization dependence of the cross peaks provides the strongest experimental evidence of large angular jumps induced by H-bond exchange. Alternatively, we can fit the peak volumes of 2D spectra to get the exchange parameters. The method of extracting the peak volumes from a 2D spectrum has been presented elsewhere.[16] As will be discussed in Sec. III, the exchange rate can be more accurately obtained from the cross peak volumes obtained from the isotropic 2DIR spectra, since this removes the orientational dynamics from the signal and makes the analysis less sensitive to spectral diffusion induced changes in the peak shapes. Once the exchange rate has been extracted from the isotropic signal, we can better determine the jump angle Θ

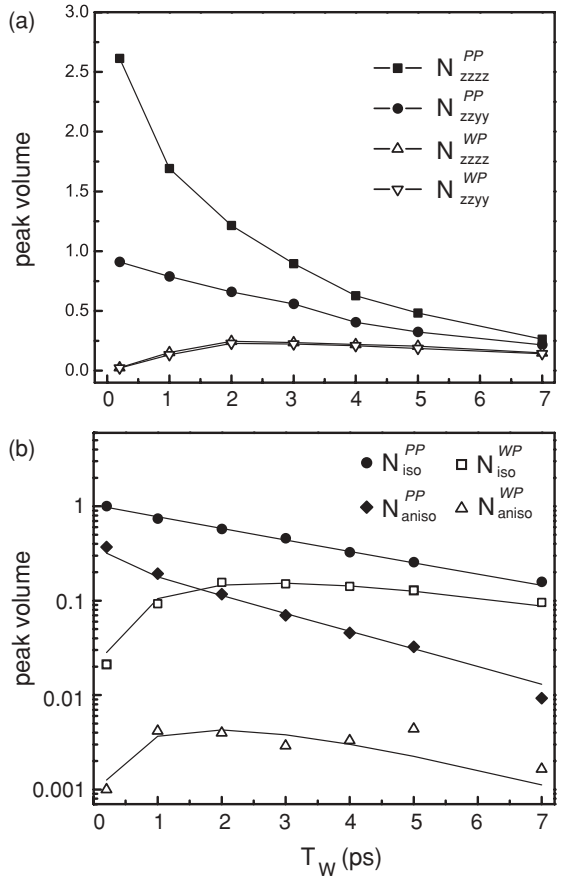

FIG. 3. Extracted peak volumes from polarization-selective 2DIR spectra. (a) Peak volumes for the diagonal peak N^{PP}_{llmm} and cross peak N^{WP}_{llmm}. While the diagonal peak intensity has a large polarization dependence, the cross peak intensity shows little polarization dependence. (b) Logarithmic plot of the peak volumes for the isotropic, $N^{ij}_{iso} = N^{ij}_{zzzz} + 2N^{ij}_{zzyy}$, and anisotropic, $N^{ij}_{aniso} = N^{ij}_{zzzz} - N^{ij}_{zzyy}$, signals for diagonal and cross peak. The solid lines give the kinetic model fit to the data with a H-bond exchange rate of 6 ± 1 ps and a jump angle of $49^\circ \pm 5^\circ$.

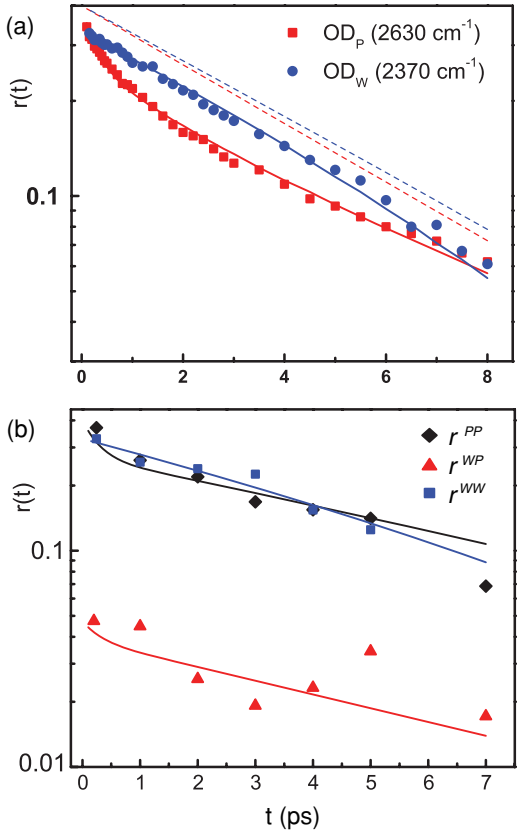

FIG. 4. Anisotropy data analysis. (a) Polarization resolved pump-probe measurements of the OD_W and OD_P final state ensemble orientational dynamics (dots). Solid lines are the best fit of the wobbling in a cone corrected JEK model [Eqs. (20)–(23)]. Dashed lines represent the JEK model with constant diffusion rates, which mismatch the data significantly. (b) 2DIR anisotropy data generated from the peak volumes of the diagonal and cross peaks (symbols). Solid lines are calculated with the wobbling in a cone corrected JEK model.

from the cross peak volumes extracted from the anisotropic 2DIR spectra. Figure 3(a) shows the polarization dependent peak volumes for the diagonal and cross peak and Fig. 3(b) shows the isotropic and anisotropic peak volumes and the fit using the model that will be discussed in Sec. III.

Polarization-selective 2DIR provides a unique way to measure the anisotropy dynamics of both intraconfigurational hydroxyl groups (diagonal peaks) and those hydroxyl groups that undergo interconfigurational H-bond exchange (cross peaks). For a broadband pump-probe measurement that excites both the OD_W and OD_P configurations, the anisotropy will reflect the orientational dynamics of both diagonal and cross peaks. This occurs because polarization-selective pump probe measurements integrate all initital frequencies, ω_τ, that contribute to the 2DIR spectrum with the same final frequency, ω_m. While the cross peaks make a comparatively small contribution to the pump-probe signal, our prior analysis of the pump probe anisotropy assumed that interconfigurational H-bond exchange did not change the anisotropy. This generates error in the OD_W and OD_P orientational time constants published previously.[36] The polarization-selective 2DIR measurement alleviates this weakness of the pump-probe measurement, but with a significant reduction in the signal-to-noise ratio. We utilize the strengths of both measurements and minimize their weaknesses by simultaneously fitting both data sets. Figure 4(a) shows the anisotropy data extracted from the pump-probe measurements and Fig. 4(b) shows the anisotropy data for different peak regions extracted from the 2DIR spectra. Since the OD_W-to-OD_P cross peak originating from the 1–2 vibrational transition overlaps with the OD_W 0–1 diagonal peak in the 2DIR spectra, we extracted the anisotropy data for the OD_W configuration from the 1–2 transition. This data came from a separate experiment with the central frequency of the laser set to 2490 cm^{-1} to better cover the OD_W 1–2 transition. The 2DIR spectra of this data set appear in Fig. 5. As expected, separation of the cross peak contribution to the anisotropy from the diagonal contribution leads to the assignment of slower intraconfigurational orientational relaxation. This further supports the conclusion from our prior experimental and simulation studies that the average orientational dynamics of all hydroxyl groups, independent of the H-bond configuration, occur more slowly than in water. This finding contradicts that of Omta *et al.*, where they found that the orientational dynamics of the OD_W configuration could not be distinguished from those of

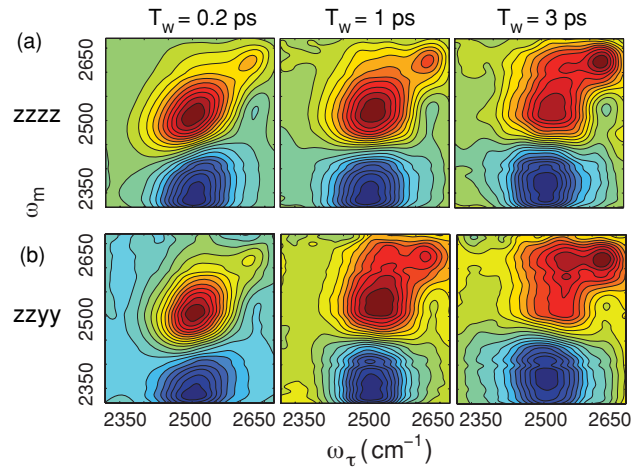

FIG. 5. Polarization-selective 2DIR spectra using IR pulses centered at 2490 cm^{-1}. These measurements emphasize the anisotropy of the OD_W configuration, particularly for the 1–2 excited state absorption.

isotopically mixed water. The discussion of differences in these measurements will be addressed in Sec. IV.

III. JUMP-EXCHANGE THEORY FOR 2DIR SPECTROSCOPY

A. Angular jump contribution to orientational relaxation

We begin with the diffusive reorientation case. The Debye model for the orientational dynamics of molecules in isotropic media assumes that the molecules rotate through very small angles before suffering an angular momentum altering collision.[29,30] We can therefore treat molecules as diffusive rotors following the diffusion equation,

$$\frac{\partial}{\partial t}\rho(\Omega,t) = D_{\mathrm{or}}\nabla_{\Omega}^{2}\rho(\Omega,t), \tag{1}$$

where $\Omega = (\theta,\phi)$ is the spherical coordinate of the transition dipole moment orientation, $\hat{\mu}$, of the specific IR active vibrational mode being probed, $\rho(\Omega,t)$ is the angular distribution function representing the probability of finding the dipole oriented in Ω at time t, D_{or} is the rotational diffusion coefficient, and $\nabla_{\Omega}^{2} = (1/\sin\theta)(\partial/\partial\theta)(\sin\theta(\partial/\partial\theta)) + (1/\sin^{2}\theta)(\partial^{2}/\partial\phi^{2})$ is the angular Laplacian, having spherical harmonic eigenfunctions. Since we are working on a particular dipole transition of a molecule, we apply the linear rotor assumption, and D_{or} is a scalar constant, thus the linear rotor diffuses isotropically on the surface of a unit sphere.[30] To solve this differential equation, we expand the angular distribution function in a series of spherical harmonics, assuming an initial azimuthally symmetric angular distribution $\rho(\Omega,0)$:

$$\rho(\Omega,t) = \sum_{l} C_{l}(t)Y_{l0}(\Omega)\int d\Omega_{0}Y_{l0}(\Omega_{0})\rho(\Omega_{0}). \tag{2}$$

The time coefficient $C_l(t)$ determines the time evolution of each spherical harmonic component, l, and is well known as the dipole–dipole correlation function, $C_l(t) = \langle P_l[\hat{\mu}(0)\cdot\hat{\mu}(t)]\rangle$. The initial conditions imply that $C_l(0) = 1$, and the normalization of $\rho(\Omega,t)$ requires $C_0(t) \equiv 1$.

Equation (2) works for an arbitrary azimuthally symmetric initial distribution. Linearly polarized excitation generates an initial angular distribution of $\rho(\Omega_0) = (3/4\pi)\cos^{2}\theta = (1/\sqrt{4\pi})[Y_{00}(\Omega_0) + \sqrt{4/5}Y_{20}(\Omega_0)]$, which we insert into Eq. (2) to express the time dependent angular distribution as

$$\rho(\Omega,t) = \frac{1}{\sqrt{4\pi}}\left[Y_{00} + \sqrt{\frac{4}{5}}Y_{20}(\Omega)C_{2}(t)\right]. \tag{3}$$

This result indicates that the angular distribution function contains a static isotropic term and a second d_{z^2}-orbital-like distribution with time dependent amplitude. The detailed form of the time coefficients $C_l(t)$ depends on the specific kinetic model. For the diffusive model in Eq. (1), the solution gives l-dependent time evolution coefficients equal to

$$C_{l}(t) = \exp[-l(l+1)D_{\mathrm{or}}t]. \tag{4}$$

For cases where small molecules reorient through stepwise angular jumps—the angular analogue of a translational random walk—the diffusion equation (1) is no longer valid,[30,33] but the collective behavior of the Brownian motion can be closely related to the diffusion equation. Assuming the random angular jumps have azimuthal symmetry with respect to the initial dipole orientation, as shown in Fig. 1(b), we construct a kinetic equation describing the dynamic behavior of the angular distribution function using a relaxation method,

$$\frac{\partial}{\partial t}\rho(\Omega,t) = -k_{\mathrm{jump}}\rho(\Omega,t) + \frac{k_{\mathrm{jump}}}{2\pi}\int d\Omega'\delta(\hat{\mu}\cdot\hat{\mu}' - \cos\Theta)\rho(\Omega',t), \tag{5}$$

where $k_{\mathrm{jump}} = \tau_{\mathrm{jump}}^{-1}$ is the rate of the rotational jumps, and Θ is the jump angle. The first term on the right-hand side is the loss of the probability density due to events where the vibrational transition dipole moment jumps away from the orientation, Ω, and the second term is the source of the probability density due to jumps into Ω from the surrounding cone of Ω' with the semiangle of Θ, constrained by the Dirac delta function. Using the same spherical harmonic expansion (2) to solve Eq. (5) requires solving the cone integral,

$$\begin{aligned}\frac{1}{2\pi}\int d\Omega'\delta(\hat{\mu}\cdot\hat{\mu}' - \cos\Theta)\mathrm{Y}_{l0}(\Omega') &= \frac{1}{2\pi}\int d\Omega'\sum_{m'}D^{l}_{m'0}(0,\theta,0)\delta(\cos\theta' - \cos\Theta)\mathrm{Y}_{lm'}(\Omega') \\ &= P_{l}(\cos\Theta)\mathrm{Y}_{l0}(\Omega),\end{aligned} \tag{6}$$

where $D^{l}_{m'0}$ is the Wigner D-matrix,[40] and $P_l(\cos\Theta)$ is the Legendre function. The physical interpretation of Eq. (6) is clear; angular jumps simply redistribute the initial density $\mathrm{Y}_{l0}(\Omega)$ by a factor of $P_l(\cos\Theta)$. The detailed integration method can be found in the supporting online information.[41] The solution of the kinetic Eq. (5) gives

$$C_{l}(t) = \exp\{-k_{\mathrm{jump}}t[1 - P_{l}(\cos\Theta)]\}. \tag{7}$$

Comparing the results of Eqs. (4) and (7), we can connect the diffusion rate with the dynamical properties including the jump rate and jump angle. Notice that when Θ is very small, $P_l(\cos\Theta) \simeq 1 - l(l+1)\Theta^{2}/4$ and the jump model converges

to the diffusion model, since the Debye model is a small-step diffusion model. The relation between the parameters is

$$D_{\text{or}} = \frac{\Theta^2}{4} k_{\text{jump}}. \tag{8}$$

This result is identical to the extended diffusion model developed by Berne and Pecora,[30] but differs from Ivanov's model[33] by a factor of 3/2. The discrepancy comes from Ivanov's use of a spherical rotor instead of a linear rotor approximation. Ivanov's model does not constrain the jumps to a cone, and therefore might not be as applicable to nonlinear spectroscopies where the involved transition dipoles are better approximated by linear rotors. The result of Eq. (7) indicates that the large angular jump reorientation results in different diffusion constants for spherical harmonic components with different angular momenta.

Equation (5) acts like a Green's function, assuming all jump events have the same value of jump angle Θ. In reality, angular jumps will occur with a range of Θ represented by the distribution function $\zeta(\Theta)$. We can rewrite the kinetic equation as,

$$\begin{aligned}\frac{\partial}{\partial t}\rho(\Omega, t) = &-k_{\text{jump}}\rho(\Omega, t) \\ &+ \frac{k_{\text{jump}}}{2\pi}\int d\Theta\zeta(\Theta) \\ &\times \int d\Omega'\delta(\hat{\mu}\cdot\hat{\mu}' - \cos\Theta)\rho(\Omega', t).\end{aligned} \tag{9}$$

As a consequence of Eq. (9), the corresponding results need to replace $P_l(\cos\Theta)$ with the ensemble averaged value $\langle P_l(\cos\Theta)\rangle = \int d\Theta\zeta(\Theta)P_l(\cos\Theta)$.

For anisotropic third order nonlinear spectroscopic measurements like polarization-selective pump-probe and 2DIR spectroscopy, we only access $l = 0, 2$. For pump-probe, the parallel and perpendicular projection of the third order orientational response function can be calculated by ensemble averaging:

$$\begin{aligned}R_{zzzz}(t) &= \int d\Omega\rho(\Omega, t)\cos^2\theta = \frac{1}{3}\left[1 + \frac{4}{5}C_2(t)\right], \\ R_{zzyy}(t) &= \int d\Omega\rho(\Omega, t)\sin^2\theta\cos^2\phi \\ &= \frac{1}{3}\left[1 - \frac{2}{5}C_2(t)\right].\end{aligned} \tag{10}$$

These response functions can be used to calculate the anisotropy,

$$r(t) = \frac{R_{zzzz}(t) - R_{zzyy}(t)}{R_{zzzz}(t) + 2R_{zzyy}(t)} = \frac{2}{5}C_2(t) = \frac{2}{5}\exp\left(-t/\tau_{\text{or}}\right). \tag{11}$$

While $C_2(t)$ is generally a multiexponential function determined by the overall dynamics of the three reorientation pathways discussed in the Introduction, we can still see the effect of the individual pathway. We mainly discuss rotational diffusion and angular jumps in the present section, and correct the contribution of librational motion in a later section. If diffusion is the dominant source of molecule reorientation, the anisotropy decays monoexponentially with a decay time constant of $\tau_{\text{or}} = (6D_{\text{or}})^{-1}$, as seen in Eq. (4). If the orientational relaxation is dominated by angular jumps, there is a simple relationship between the jump rate and the orientational relaxation time, τ_{or},

$$\tau_{\text{or}} = \tau_{\text{jump}}\left[1 - \langle P_2(\cos\Theta)\rangle\right]^{-1} \tag{12}$$

where $P_2(\cos\Theta) = (3\cos^2\Theta - 1)/2$. Notice that when molecules jump by the magic angle ($\Theta_{\text{magic}} = 54.7^\circ$), the orientational relaxation rate equals the angular jump rate. Usually the orientational motion of molecules involve both small angle diffusion and large angular jumps, such as the diffusive reorientation of the OD$\cdots$O–H-bond and large angular jumps associated with hydroxyl group H-bond switching.[4] For most cases, we cannot distinguish between the two processes; however, both processes lead to mono-exponential orientational relaxation, so the combined effect remains single exponential, $C_2^{\text{total}}(t) = C_2^{\text{diff}}(t)C_2^{\text{jump}}(t)$. This allows both diffusion and angular jump rotation within a given H-bond configuration to be effectively described with a single diffusion equation using an effective diffusion constant.[7] Thus in the discussion below of the jump exchange kinetic model, we keep the diffusion equation to account for the total orientational motion within each H-bond configuration, where it is not possible to unambiguously distinguish jump angle rotation associated with intraconfigurational H-bond exchanges and orientational diffusion with a fixed H-bond. Note that 2DIR spectroscopy only resolves the interconfigurational H-bond switching since this generates a change in vibrational frequency.

B. Angular jump-exchange kinetic (JEK) model for 2DIR spectroscopy

Chemical exchange induced angular jumps have a large impact on the polarization-selective 2DIR spectra. As shown by Ji *et al.*, the very weak anisotropy of the cross peak intensity in aqueous $NaClO_4$ solution is the effect of large angular jumps of the hydroxyl stretch transition dipole moment induced by H-bond exchange.[9] In order to quantitatively analyze the experimental 2D spectra, we provide a jump-exchange model without considering the librational motion of molecules for simplicity. In a later section, we will integrate the librational motion into our JEK model using a wobbling in a cone model. Assuming the chemical exchange of two conformations with an angular jump of Θ, we model the orientational contribution of each configuration with the intraconfigurational diffusion equation constructed in Sec. III A; the gain of population density at the orientation Ω is modeled by the jump conversion from the other hydroxyl group H-bond configuration with orientations of Ω' forming a cone of semiangle Θ with respect to Ω. The model assumes an instantaneous change in angle upon H-bond exchange. This approximation will have minimal effect on the analysis as long as the rate of the reorientation associated with the jump proceeds much more quickly than the rate of H-bond switching. The loss of density due to the population relaxation of each configuration and the chemical conversion to the other configuration is modeled using the approach of Kwak *et al.*[16] For the aqueous $NaClO_4$ system,

the coupled differential equations are constructed to be

$$\frac{\partial}{\partial t}[N_{\mathrm{W}}(t)\rho_{\mathrm{W}}(\Omega,t)] = -(k_{\mathrm{W}} + k_{\mathrm{W-P}} - D_{\mathrm{W}}\nabla_{\Omega}^2)[N_{\mathrm{W}}(t)\rho_{\mathrm{W}}(\Omega,t)] + \frac{k_{\mathrm{P-W}}}{2\pi}\int d\Omega'\delta(\hat{\mu}\bullet\hat{\mu}' - \cos\Theta)[N_{\mathrm{P}}(t)\rho_P(\Omega',t)],$$
$$\frac{\partial}{\partial t}[N_{\mathrm{P}}(t)\rho_{\mathrm{P}}(\Omega,t)] = -(k_{\mathrm{P}} + k_{\mathrm{P-W}} - D_{\mathrm{P}}\nabla_{\Omega}^2)[N_{\mathrm{P}}(t)\rho_{\mathrm{P}}(\Omega,t)] + \frac{k_{\mathrm{W-P}}}{2\pi} \times \int d\Omega'\delta(\hat{\mu}\bullet\hat{\mu}' - \cos\Theta)[N_{\mathrm{W}}(t)\rho_{\mathrm{W}}(\Omega',t)]. \quad (13)$$

In this jump-exchange kinetic model, $N_i(t)$ represents the population density for the excited state hydroxyl groups in a water–water H-bond configuration ($i = \mathrm{W}$) and those hydroxyl groups in a water-perchlorate H-bond configuration ($i = \mathrm{P}$). The model attributes the dynamics to population decay with decay rates k_i, orientational relaxation within configuration i with the effective diffusion constant D_i, and chemical exchange with rate constant k_{i-j}, and a H-bond exchange jump angle Θ. As mentioned above, the intraconfigurational reorientation is still modeled by an effective diffusion equation, and the interconfigurational angular jump-exchange is expressed by the integral over a cone.

Applying the spherical harmonic expansion (2) for the angular distribution function gives

$$N_i(t)\rho_i(\Omega,0) = \sum_l N_i(t)C_l^i(t)Y_{l0}(\Omega) \times \int d\Omega_0 Y_{l0}(\Omega_0)\rho_i(\Omega_0). \quad (14)$$

We insert Eq. (14) into differential equation (13), remove the Ω variable, reduce the above differential equations to equations of $N_i(t)C_l^i(t)$, and apply the result of Eq. (6) to generate

$$\frac{d}{dt}\begin{pmatrix} N_{\mathrm{W}}(t)C_l^{\mathrm{W}}(t) \\ N_{\mathrm{P}}(t)C_l^{\mathrm{P}}(t)\end{pmatrix} = -\begin{pmatrix} k_{\mathrm{W}} + k_{\mathrm{W-P}} + l(l+1)D_{\mathrm{W}} & -k_{\mathrm{P-W}}\langle P_l(\cos\Theta)\rangle \\ -k_{\mathrm{W-P}}\langle P_l(\cos\Theta)\rangle & k_{\mathrm{P}} + k_{\mathrm{P-W}} + l(l+1)D_{\mathrm{P}}\end{pmatrix}\begin{pmatrix} N_{\mathrm{W}}(t)C_l^{\mathrm{W}}(t) \\ N_{\mathrm{P}}(t)C_l^{\mathrm{P}}(t)\end{pmatrix}. \quad (15)$$

This can be solved analytically. Recalling the initial conditions for linear polarized light excitation, only $l = 0, 2$ generate nonvanishing terms. Ensemble averaging for different laser polarizations gives: $(N_i(t))_{zzzz} = \int d\Omega[N_i(t)\rho_i(\Omega,t)]\cos^2\theta$ and $(N_i(t))_{zzyy} = \int d\Omega[N_i(t)\rho_i(\Omega,t)]\sin^2\theta\cos^2\phi$. The population contributions to the third order nonlinear signal with parallel ($zzzz$) and perpendicular ($zzyy$) polarization geometries equal,

$$\begin{pmatrix} N_{\mathrm{W}}(t) \\ N_{\mathrm{P}}(t)\end{pmatrix}_{zzzz} = \left(e^{-\mathbf{A}\cdot t} + \frac{4}{5}e^{-\mathbf{B}\cdot t}\right)\times\frac{1}{3}\begin{pmatrix} N_{\mathrm{W}}(0) \\ N_{\mathrm{P}}(0)\end{pmatrix},$$
$$\begin{pmatrix} N_{\mathrm{W}}(t) \\ N_{\mathrm{P}}(t)\end{pmatrix}_{zzyy} = \left(e^{-\mathbf{A}\cdot t} - \frac{2}{5}e^{-\mathbf{B}\cdot t}\right)\times\frac{1}{3}\begin{pmatrix} N_{\mathrm{W}}(0) \\ N_{\mathrm{P}}(0)\end{pmatrix}, \quad (16)$$

where,

$$\mathbf{A} = \begin{pmatrix} k_{\mathrm{W}} + k_{\mathrm{W-P}} & -k_{\mathrm{P-W}} \\ -k_{\mathrm{W-P}} & k_{\mathrm{P}} + k_{\mathrm{P-W}}\end{pmatrix} \quad \text{and}$$
$$\mathbf{B} = \begin{pmatrix} k_{\mathrm{W}} + k_{\mathrm{W-P}} + 6D_{\mathrm{W}} & -\langle P_2(\cos\Theta)\rangle k_{\mathrm{P-W}} \\ -\langle P_2(\cos\Theta)\rangle k_{\mathrm{W-P}} & k_{\mathrm{P}} + k_{\mathrm{P-W}} + 6D_{\mathrm{P}}\end{pmatrix}.$$

Equation (16) can be used to construct the isotropic and anisotropic contributions to the populations

$$\begin{pmatrix} N_{\mathrm{W}}(t) \\ N_{\mathrm{P}}(t)\end{pmatrix}_{\mathrm{iso}} = \begin{pmatrix} N_{\mathrm{W}}(t) \\ N_{\mathrm{P}}(t)\end{pmatrix}_{zzzz} + 2\begin{pmatrix} N_{\mathrm{W}}(t) \\ N_{\mathrm{P}}(t)\end{pmatrix}_{zzyy} = e^{-\mathbf{A}\cdot t}\times\begin{pmatrix} N_{\mathrm{W}}(0) \\ N_{\mathrm{P}}(0)\end{pmatrix},$$
$$\begin{pmatrix} N_{\mathrm{W}}(t) \\ N_{\mathrm{P}}(t)\end{pmatrix}_{\mathrm{aniso}} = \begin{pmatrix} N_{\mathrm{W}}(t) \\ N_{\mathrm{P}}(t)\end{pmatrix}_{zzzz} - \begin{pmatrix} N_{\mathrm{W}}(t) \\ N_{\mathrm{P}}(t)\end{pmatrix}_{zzyy} = \frac{2}{5}e^{-\mathbf{B}\cdot t}\times\begin{pmatrix} N_{\mathrm{W}}(0) \\ N_{\mathrm{P}}(0)\end{pmatrix}. \quad (17)$$

These results extend the polarization dependent signal of a single chemical conformer to two interconverting conformers, expanding the experimental observable from a scalar to a vector. Notice the similarity between Eqs. (10) and (16), with the kinetic information embedded in **A** and **B** matrices. The **A** matrix has no orientational dependence and contributes solely to the isotropic response with dynamics determined by the excited state lifetime and the chemical exchange rate. The **B** matrix contributes solely to the anisotropic response with additional dynamics determined by Θ, D_{W}, and D_{P}. As expected, when $\Theta = 0$, the JEK model reduces to the result of Kwak *et al.*[16] In the supporting online information[41] we discuss the relationship between the JEK model and Golonzka's theory of coupled vibrational transition dipoles.[35]

We have deduced the polarization dependent ensemble averaged population response. In order to obtain the optical response, we need to introduce transition dipole moments μ_i, since third order nonlinear signal is proportional to $|\mu_i|^2|\mu_j|^2$. For polarization-selective 2DIR spectroscopy, we use density matrices $\mathbf{N}_{llmm}(t)$ with matrix elements $N^{ij}_{llmm}(t)$ representing the populations of the diagonal ($i = j$) and cross peaks ($i \neq j$) in 2DIR spectra with parallel ($llmm = zzzz$) and perpendicular ($llmm = zzyy$) polarization geometries,

$$\mathbf{N}_{zzzz}(t) = \frac{1}{3}\begin{pmatrix} |\mu_{\mathrm{W}}|^2 & 0 \\ 0 & |\mu_{\mathrm{P}}|^2 \end{pmatrix}\left(e^{-\mathbf{A}\cdot t} + \frac{4}{5}e^{-\mathbf{B}\cdot t}\right) \times \begin{pmatrix} |\mu_{\mathrm{W}}|^2 & 0 \\ 0 & |\mu_{\mathrm{P}}|^2 \end{pmatrix}\begin{pmatrix} N_{\mathrm{W}}(0) & 0 \\ 0 & N_{\mathrm{P}}(0) \end{pmatrix},$$
$$\mathbf{N}_{zzyy}(t) = \frac{1}{3}\begin{pmatrix} |\mu_{\mathrm{W}}|^2 & 0 \\ 0 & |\mu_{\mathrm{P}}|^2 \end{pmatrix}(e^{-\mathbf{A}\cdot t} - \frac{2}{5}e^{-\mathbf{B}\cdot t}) \times \begin{pmatrix} |\mu_{\mathrm{W}}|^2 & 0 \\ 0 & |\mu_{\mathrm{P}}|^2 \end{pmatrix}\begin{pmatrix} N_{\mathrm{W}}(0) & 0 \\ 0 & N_{\mathrm{P}}(0) \end{pmatrix}. \quad (18)$$

Equation (18) is the product of four matrices representing (from right to left) the initial density matrix, the field–dipole interaction of the first two pulses, the time evolution of the populations during the waiting time period, T_{W}, and the field–dipole interaction of the third pulse and the final dipole emitting the detected signal. As pointed out by Kwak *et al.*,[16] chemical exchanges in the coherence periods do not contribute to the cross peaks in 2DIR spectra, thus only the dynamics in the waiting time is considered for population evolution. However, dephasing dynamics in coherence periods are very important for peak shapes and spectral diffusion, which are well modeled by the vibrational response functions.

For 1D polarization-selective pump-probe spectra, we use a vector $\mathbf{I}_{llmm}(t)$ with components $I^i_{llmm}(t)$ representing the peak intensity of each species i. According to the projection theorem,

$$\mathbf{I}_{zzzz}(t) = \frac{1}{3}\begin{pmatrix} |\mu_{\mathrm{W}}|^2 & 0 \\ 0 & |\mu_{\mathrm{P}}|^2 \end{pmatrix}\left(e^{-\mathbf{A}\cdot t} + \frac{4}{5}e^{-\mathbf{B}\cdot t}\right) \times \begin{pmatrix} |\mu_{\mathrm{W}}|^2 & 0 \\ 0 & |\mu_{\mathrm{P}}|^2 \end{pmatrix}\begin{pmatrix} N_{\mathrm{W}}(0) \\ N_{\mathrm{P}}(0) \end{pmatrix},$$
$$\mathbf{I}_{zzyy}(t) = \frac{1}{3}\begin{pmatrix} |\mu_{\mathrm{W}}|^2 & 0 \\ 0 & |\mu_{\mathrm{P}}|^2 \end{pmatrix}\left(e^{-\mathbf{A}\cdot t} - \frac{2}{5}e^{-\mathbf{B}\cdot t}\right) \times \begin{pmatrix} |\mu_{\mathrm{W}}|^2 & 0 \\ 0 & |\mu_{\mathrm{P}}|^2 \end{pmatrix}\begin{pmatrix} N_{\mathrm{W}}(0) \\ N_{\mathrm{P}}(0) \end{pmatrix}. \quad (19)$$

These results allow the extraction of the exchange dynamics and the jump-exchange mechanism from polarization-selective 2DIR and pump-probe measurements. In particular, the isotropic component can be used to extract the population lifetime and the exchange rate, and the anisotropic response can be used to get the orientational diffusion constants and the jump angle Θ.

C. Embedding wobbling in a cone librational dynamics into the JEK model

While conceptually valuable, the orientational dynamics of water molecules that remain within a particular H-bond configuration deviate from the almost single exponential behavior generated by the JEK model. This deviation is believed to result from the sub-ps librational motion of water hydroxyl groups, which can be addressed with a wobbling in a cone model.[31,32] We have extended the JEK model to include wobbling in a cone biexponential orientational dynamics within each H-bond configuration, while leaving the angular jump dynamics associated with a H-bond configuration switch unchanged. This model provides an accurate parameterization of the water orientational dynamics observed in multiple experiments[5,6,42–44] and confirms the insensitivity of the extracted jump angle to the details of the modeling.

The wobbling in a cone extension of the JEK model assumes that the wobbling motion is independent of other motions, such as the chemical exchange. The wobbling model[23,24] represents the time dependent dipole–dipole correlation function as a product of a wobbling term $C_2^{\mathrm{wob}}(t)$ and an orientation diffusion term $e^{-6D_{\mathrm{or}}t}$:

$$C_2(t) = e^{-6D_{\mathrm{or}}t}C_2^{\mathrm{wob}}(t). \quad (20)$$

In order to embed wobbling in the kinetic differential equations, we parameterize Eq. (20) into a diffusion equation with an effective time-dependent diffusion rate $D_{\mathrm{eff}}(t)$

$$\frac{d}{dt}C_2(t) = -6D_{\mathrm{eff}}(t)C_2(t),$$
$$6D_{\mathrm{eff}}(t) = 6D_{\mathrm{or}} - \frac{d}{dt}\ln[C_2^{\mathrm{wob}}(t)]. \quad (21)$$

Now we replace the diffusion constant in differential equations (13) with Eq. (21). Following the same procedures discussed previously, we get a result with the same form as (16), with the only change being in the **B** matrix, which is now time dependent. Generally we need to solve Eq. (15) numerically, and use it in the numerical calculation of 2DIR spectra. However, if the wobbling is so much faster than diffusion that the coefficient matrix in Eq. (15) quickly becomes constant, then an approximate analytical solution can be achieved by directly integrating the coefficient matrix to get

$$\mathbf{B}(t) = \begin{pmatrix} k_{\mathrm{W}} + k_{\mathrm{W-P}} + 6D_{\mathrm{W}} - \ln[C_{2\mathrm{W}}^{\mathrm{wob}}(t)]/t & -\langle P_2(\cos\Theta)\rangle k_{\mathrm{P-W}} \\ -\langle P_2(\cos\Theta)\rangle k_{\mathrm{W-P}} & k_{\mathrm{P}} + k_{\mathrm{P-W}} + 6D_{\mathrm{P}} - \ln[C_{2\mathrm{P}}^{\mathrm{wob}}(t)]/t \end{pmatrix}. \quad (22)$$

The strict solution of the wobbling in a cone model is a sum of over an infinite number of exponentials.[23,24] Here we use an approximate result widely accepted in treating water orientational dynamics, $C_2^{\text{wob}}(t) = S^2 + (1 - S^2)e^{-t/\tau_{\text{eff}}}$. S and τ_{eff} are new fitting parameters included to fit both the 2DIR peak volumes and the pump-probe data. The order parameter $S = \cos\theta_c(1 + \cos\theta_c)/2$, where θ_c is the cone semi-angle. Notice that although wobbling motion causes a very fast decay of orientational memory, the amplitude of this decay component is relatively small (~20%). In other words, fast librational motion only partially scrambles the orientational memory. This is seen more clearly in Sec. III D where we formulate the anisotropy dynamics explicitly, so that the contribution of the three pathways to orientational memory can be compared easily.

D. Anisotropy in 2DIR spectra

Since there are multiple mechanisms for the OD transition dipole moment to lose orientational memory, it is necessary to have a qualitative view of the contribution of each reorientational pathway to the anisotropy of different peak regions in the 2D spectra, and show the unique effect of large angular jumps in reducing the anisotropy of the cross peaks associated with H-bond configurational exchange. For each peak in the 2D spectra, the anisotropy can be calculated from Eq. (18) from the appropriate matrix element, $N^{ij}_{llmm}(t)$:

$$r^{ij}(t) = \frac{N^{ij}_{zzzz}(t) - N^{ij}_{zzyy}(t)}{N^{ij}_{zzzz}(t) + 2N^{ij}_{zzyy}(t)} = \frac{2}{5}\frac{[e^{-\mathbf{B}\cdot t}]_{ij}}{[e^{-\mathbf{A}\cdot t}]_{ij}}, \qquad i, j = W, P. \tag{23}$$

For the JEK model discussed above, the anisotropy of a diagonal (ij = PP) and a cross peak (ij = WP) volume equals,

$$\begin{aligned} r^{\text{PP}}(t) &= \frac{2}{5}e^{-(6D_{\text{W}}+6D_{\text{P}})t/2}F^{\text{PP}}_{\text{jump}}(t), \\ r^{\text{WP}}(t) &= \frac{2}{5}\langle P_2(\cos\Theta)\rangle\, e^{-(6D_{\text{W}}+6D_{\text{P}})t/2}F^{\text{WP}}_{\text{jump}}(t). \end{aligned} \tag{24}$$

The anisotropy of the 2DIR peak volumes with the wobbling correction equals,

$$\begin{aligned} r^{\text{PP}}(t) &= \frac{2}{5}\sqrt{C^{\text{wob}}_{2\text{P}}(t)C^{\text{wob}}_{2\text{W}}(t)} \\ &\quad \times e^{-(6D_{\text{W}}+6D_{\text{P}})t/2}F^{\text{PP}}_{\text{wob}}(t), \\ r^{\text{WP}}(t) &= \frac{2}{5}\langle P_2(\cos\Theta)\rangle\sqrt{C^{\text{wob}}_{2\text{P}}(t)C^{\text{wob}}_{2\text{W}}(t)} \\ &\quad \times e^{-(6D_{\text{W}}+6D_{\text{P}})t/2}F^{\text{WP}}_{\text{wob}}(t), \end{aligned} \tag{25}$$

where the $F^{ij}(t)$ are complicated functions of time and involve cosh and sinh functions of the **A** and **B** matrix elements, with $F^{ij}(0) = 1$. Nonetheless, because the rotational time constants of the two hydroxyl configurations do not differ significantly in our particular system (see Table I), $F^{ij}(t)$ functions have sufficiently weak time dependence so that they can be approximated as time independent to assist our qualitative discussion. The detailed form of $F^{ij}(t)$ can be found in the supporting online information.[41] We can see the anisotropy of both diagonal and cross peaks relax with a rate dictated by a mean diffusion constant, and modified by the $F^{ij}(t)$ functions. The angular jump only has direct impact on the anisotropy of the cross peak, reducing the anisotropy of the cross peak by a factor of $\langle P_2(\cos\Theta)\rangle$, while the diagonal peak anisotropy remains almost unchanged. In the systems where chemical exchange preserves the transition dipole moment orientation, $\Theta = 0^\circ$ and $P_2(\cos\Theta) = 1$, the diagonal and cross peaks have similar anisotropy. However, when the angular jump is large, such as $\Theta = 50^\circ$and $P_2(\cos\Theta) = 0.12$, the cross peak anisotropy r^{WP} will be greatly reduced. Thus, analyzing the relative anisotropy of the diagonal and cross peaks provides direct information about the jump angle.

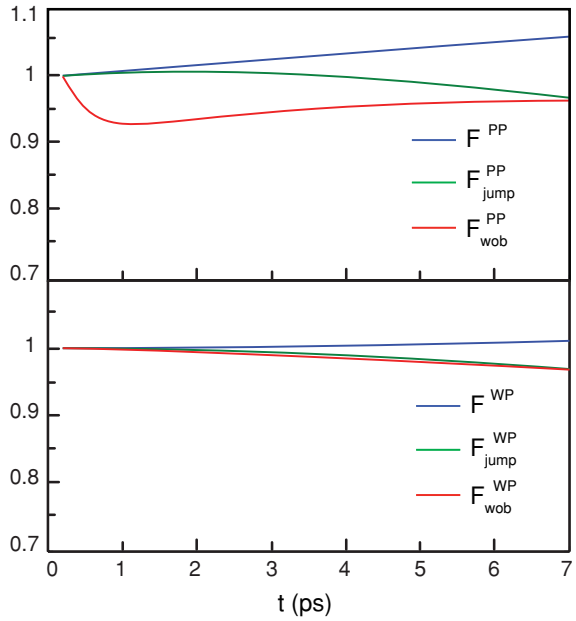

FIG. 6. $F^{ij}(t)$ functions calculated using the parameters from the best fit results. The blue lines represent $F^{ij}(t)$ calculated from the JEK model without angular jump ($\Theta = 0$), green and red lines represent $F^{ij}_{\text{jump}}(t)$ and $F^{ij}_{\text{wob}}(t)$ calculated from JEK and wobbling corrected JEK model, respectively, with $\Theta = 50^\circ$. Note that these functions always reside within 10% of unity, validating their exclusion from the qualitative discussion.

The librations have similar effects on the diagonal and cross peak anisotropy, which contain a mean wobbling orientational relaxation $\sqrt{C^{\text{wob}}_{2\text{P}}(t)C^{\text{wob}}_{2\text{W}}(t)}$ and a $F^{ij}_{\text{wob}}(t)$ function. For the dynamic parameters extracted from both the 2DIR and pump-probe experiments, Fig. 6 shows the $F^{ij}(t)$ functions for the JEK model and the wobbling corrected JEK model. The wobbling only contributes to the fast early time decay of the $F^{ij}_{\text{wob}}(t)$ and these functions have minimal deviation from 1 within our experimental delay time. Thus the librational motions of water molecules partially scramble the anisotropy of both the diagonal and cross peaks by a factor of roughly $(1 - S^2)$, but they cannot account for the large difference between diagonal and cross peak anisotropies. Within the context of our model, only the large angular jump can explain the vanishingly small anisotropy of the cross peak.

TABLE I. Parameters extracted from the best fits of the experimental spectra to the JEK and the wobbling-corrected JEK models. The following relationships exist between the parameters in the table and those in the model: $\tau_{or} = (6D)^{-1}$, $T_1 = k^{-1}$, and $\tau_{ex} = (k_{P-W} + k_{W-P})^{-1}$.

Model	Species	τ_{or} (ps)	S^2	τ_{eff} (ps)	T_1 (ps)	Θ Θ	τ_{ex} (ps)
JEK	OD_P	4.6 ± 0.5	1	N/A	5.24	50 ± 5	5 ± 1
	OD_W	5.0 ± 0.5	1	N/A	2.54		
Wob-JEK	OD_P	8.3 ± 1	0.65	0.3	5.24	49 ± 5	6 ± 1
	OD_W	6.0 ± 1	0.83	0.03	2.54		

IV. DISCUSSION

We have developed a jump-exchange kinetic theory to include the effect of angular jump-reorientation for calculating the polarization dependence of 2DIR spectroscopic measurements. The results suggest that large angular jumps associated with changes in the hydroxyl group H-bond conformation would have very different effects on the anisotropy of the diagonal and cross peaks, making polarization-selective 2DIR a powerful experimental tool for measuring orientational changes associated with conformational changes, such as H-bond angular jump exchange or bond isomerization.[9]

In the present section we show the detailed analysis of our experimental polarization-selective 2DIR spectra, as well as polarization-selective one-dimensional infrared pump-probe spectra for 6M aqueous $NaClO_4$. The combination of the two measurements supports the large angular jump mechanism for H-bond exchange between the OD_P and OD_W configurations, and allows us to measure the orientational dynamics of water molecules within each of the two H-bond configurations.

A. Extracting the jump angle from polarization-selective 2DIR spectra

We perform response function calculations using diagrammatic perturbation theory combined with the JEK model to numerically calculate the 2DIR spectra.[16,45] By introducing the polarization-dependent orientational response $\mathbf{N}_{llmm}(t)$, we can write the overall response function as

$$S^R_{llmm}(t_3, T_W, t_1) = \sum_{\alpha=1}^{3} \sum_{i,j} N^{ij}_{llmm}(T_W) R^{ij}_{\alpha}(t_3, T_w, t_1),$$
$$S^{NR}_{llmm}(t_3, T_W, t_1) = \sum_{\alpha=4}^{6} \sum_{i,j} N^{ij}_{llmm}(T_w) R^{ij}_{\alpha}(t_3, T_W, t_1), \quad (26)$$

where R^{ij}_{α} is the vibronic response function for peak position (ω_i, ω_j) and $\alpha = 1, 2, 3$ represent the rephasing quantum pathways for the ground state bleach (GB), stimulated emission (SE), and transient absorption (TA) signals, respectively, while $\alpha = 4, 5, 6$ represent the nonrephasing quantum pathways for the corresponding GB, SE, and TA signals. Using the Condon approximation and the second-order cumulant expansion, we calculate R^{ij}_{α} following the same approach described in detail by Kwak *et al.*,[16] while the expression for $N^{ij}_{llmm}(t)$ can be found in Eq. (18).

After generating the time-domain response function, the 2D spectrum is given by

$$S_{llmm}(\omega_\tau, \omega_m, T_W) \propto \{\mathrm{Re}\}\left[\tilde{S}^R_{llmm}(\omega_\tau, \omega_m, T_W) + \tilde{S}^{NR}_{llmm}(\omega_\tau, \omega_m, T_W)\right], \quad (27)$$

where $\tilde{S}^R_{llmm}$ and $\tilde{S}^{NR}_{llmm}$ are calculated by double Fourier transformation,

$$\tilde{S}^R_{llmm}(\omega_\tau, \omega_m, T_W) = \int_0^\infty dt_1 \int_0^\infty dt_3 e^{i\omega_m t_3 - i\omega_\tau t_1} S^R_{llmm}(t_3, T_W, t_1),$$
$$\tilde{S}^{NR}_{llmm}(\omega_\tau, \omega_m, T_W) = \int_0^\infty dt_1 \int_0^\infty dt_3 e^{i\omega_m t_3 + i\omega_\tau t_1} S^{NR}_{llmm}(t_3, T_W, t_1). \quad (28)$$

The isotropic and anisotropic 2DIR spectra are defined as

$$S_{iso}(\omega_\tau, \omega_m, T_W) = S_{zzzz}(\omega_\tau, \omega_m, T_W) + 2S_{zzyy}(\omega_\tau, \omega_m, T_W),$$
$$S_{aniso}(\omega_\tau, \omega_m, T_W) = S_{zzzz}(\omega_\tau, \omega_m, T_W) - S_{zzyy}(\omega_\tau, \omega_m, T_W). \quad (29)$$

We fit the experimental 2DIR spectra with the numerical response function calculation described above. Some of the parameters can be determined from pump-probe measurements, such as the population relaxation rate k_i, or the linear absorption spectrum, such as the central frequency and spectral width of each absorption peak. We extract the orientational relaxation rate, D_i, within each H-bond configuration with a combination of the polarization-selective pump-probe and 2DIR measurements. The slower components of the frequency–frequency correlation function (FFCF) can be measured with the center line slope (CLS) method from the T_W-dependent 2DIR spectra.[46] While the rest of the parameters, including the anharmonic shift $\Delta\omega_i$, the motionally narrowed components of the FFCF, the relative equilibrium concentration, the relative transition dipole moment, the exchange rate k_{i-j}, and the jump angle Θ are varied to fit both the FTIR spectrum and the 2DIR spectra. The experimental data has been presented in Sec. II, with some of the data having been published in a previous work.[9] Figure 2 shows S_{iso} and S_{aniso} for various waiting times. The clear growth of the cross peaks in S_{iso} indicates the existence of H-bond exchange with a time constant of 6 ± 1 ps. More interestingly, the very

small amplitude of the cross peak in S_{aniso} is direct evidence of large angular jumps associated with H-bond exchange. Fitting results indicate a jump angle of $\Theta = 49 \pm 5^{\circ}$. The calculated S_{aniso} using $\Theta = 50^{\circ}$ appear in Fig. 2(c).

Alternatively, we can fit the peak volumes (N_{llmm}^{ij}) of 2D spectra to get the exchange parameters. The method of extracting the peak volumes from a 2D spectrum was presented elsewhere.[16] Equations (16) and (17) suggest that N_{iso}^{ij} can be used to extract the exchange rate more accurately without the need to manipulate D_i, Θ, and FFCF. Once the exchange rate is determined, we can better extract Θ from N_{aniso}^{ij}. Figure 3(a) shows the polarization dependent peak volumes for the diagonal and cross peak, while Fig. 3(b) shows the isotropic and anisotropic peak volumes and the fits using the parameters listed in Table I.

B. Orientational relaxation dynamics

In addition to addressing the mechanism of H-bond switching in water and aqueous solutions, the $NaClO_4$ solution also provides an excellent opportunity to assess the impact of ions on the dynamics of water molecules. The distinct hydroxyl stretch frequencies of the OD_W and OD_P configurations provide the opportunity to determine the impact of the perchlorate anion on hydroxyl group orientational relaxation, as well as determine the extent to which ions influence the orientational dynamics of hydroxyl groups participating in water–water H-bonds. The spatial extent to which an ion changes the structure and dynamics of water remains a contentious issue with one position emphasizing that most ions only significantly influence water molecules that reside in direct contact with the ions.[47] The ultrafast vibrational anisotropy measurements of Omta and Bakker in 6M $NaClO_4$ represents one of the more provocative experimental supports for the very short ranged influence of ions in aqueous solution.[43] They found that the orientational relaxation dynamics of the OD_W configuration could not be distinguished from the orientational dynamics of isotopically mixed water and concluded from this work that the ions in solution had minimal impact on the structure and dynamics of hydroxyl groups not in direct contact with an ion. In our study we observe rotational dynamics for the OD_P configuration quite similar to those of Omta *et al.*, but we observe rotational dynamics for the OD_W configuration quite distinct from those observed by Bakker and co-workers.

The analysis of the experimental measurements utilizes Eqs. (17)–(19) for fitting the polarization resolved 2DIR and pump-probe data and the fitting results can be found in Table I. Figure 5(a) shows the pump-probe anisotropy data and the fitting curves using the wobbling corrected JEK model. We use the 0–1 transition of OD_P at 2630 cm^{-1} to analyze the orientation dynamics of OD_P, and the 1–2 transition of OD_W at 2370 cm^{-1} to analyze the dynamics of OD_W to avoid spectral overlap of the two H-bond configurations. The similar value of the anisotropy measured for very early delay times in water for the 0–1 and the 1–2 transitions demonstrate the parallel direction of these two transition dipole moments. Our results show a slow orientational relaxation time for the OD_P configuration of 8.3 ± 1 ps and a slow orientational relaxation time for the OD_W configuration of 6 ± 1 ps. Our value for the orientation relaxation time for the OD_W configuration exceeds the value of Omta *et al.* by roughly a factor of 2. While not in quantitative agreement, our results qualitatively agree with the rotational correlation functions extracted from Car–Parrinello molecular dynamics simulations of aqueous 6M $NaClO_4$, where the OD_W configuration has a rotational decay time constant 60% larger than water.[36]

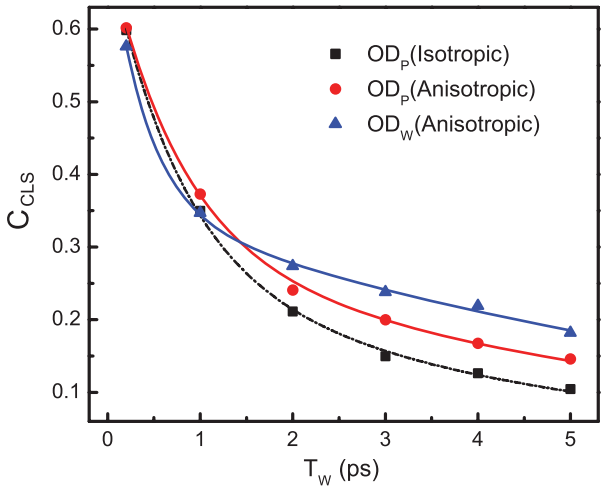

FIG. 7. CLS measurements of the normalized FFCF extracted for the OD_W diagonal peak from the anisotropic 2DIR spectra and the OD_P diagonal peak from both isotropic and anisotropic 2DIR spectra. We analyze only the anisotropic spectra for OD_W because the isotropic spectra have overlapping spectral components that preclude a robust lineshape analysis. Biexponential fitting results are shown in Table II.

Given the significance of the findings of Omta *et al.*, we have attempted to determine the origin of the discrepancy between the two measurements. The spectral bandwidth of the pump pulse represents the most significant difference between the two measurements. We have used spectrally broad pulses with bandwidths of 250 cm^{-1} FWHM, while Omta and Bakker[43] used 80 cm^{-1} FWHM pump pulses. This provides a critical distinction between the two measurements because our pump pulse spectrally overlaps most of the OD_W and OD_P absorption bands [see Fig. 1(a)], while the measurements of Bakker and co-workers preferentially excited a subset of hydroxyl groups within the OD_W or the OD_P bands. Spectrally dependent rotational dynamics within a specific H-bond configuration could explain the discrepancy between the two measurements. To investigate this hypothesis, we used the CLS method to extract the spectral diffusion dynamics of the OD_W configuration from the 2DIR spectra. The normalized FFCF for the OD_W and the OD_P configurations appear in Fig. 7. The FFCF has been extracted from the anisotropic 2DIR spectra for both H-bond configurations and only for the OD_P configuration for the isotropic signal. We cannot robustly extract the FFCF for the OD_W configuration from the isotropic 2DIR spectra because the OD_W to OD_P 1–2 cross peak overlaps the OD_W 0–1 transition and makes lineshape analysis unreliable for this signal (see Fig. 2). This does not cause a problem for the anisotropic 2DIR spectra because the cross peak has a very small anisotropy.[41]

TABLE II. Parameters extracted from the biexponential fits of the CLS data, $C_{CLS}(t) = a_1 e^{-t/\tau_1} + a_2 e^{-t/\tau_2}$.

Configuration	a_1	τ_1 (ps)	a_2	τ_2 (ps)
$OD_{P\ (iso)}$	0.45	0.75	0.26	5.3 ± 0.5
$OD_{P\ (aniso)}$	0.42	0.78	0.29	6.9 ± 0.5
$OD_{W\ (aniso)}$	0.38	0.46	0.33	7.6 ± 0.5

The spectral dynamics for both configurations occur on three time scales. The parameters extracted from the analysis of the FFCF can be found in Table II. The fastest component that wedo not resolve is a common observation for the hydroxyl stretch dynamics of water.[5,48–50] Simulations demonstrate that the memory loss associated with this component of the FFCF can be attributed to the librational motion of the hydroxyl group.[5,48] This component of the spectral response motionally narrows and does not contribute to the spectral inhomogeneity. The next fastest response proceeds on the picosecond time scale and does not have orientational dependence for the OD_P configuration. The time scale and absence of orientational dependence indicates that these spectral dynamics result from overdamped H-bond stretching dynamics. The slowest component of the response does show significant orientational dependence, with the slow component of the isotropic FFCF decaying more quickly than the slow component of the anisotropic FFCF for the OD_P configuration. The orientation dependence of the spectral diffusion dynamics indicates that the inhomogeneous broadening of the hydroxyl stretch does not originate solely from a distribution in H-bond lengths, but also H-bond angles.[50] The anisotropy of the slow spectral diffusion dynamics demonstrates that some combination of H-bond jump exchange and hydroxyl group rotational diffusion contributes to the spectral diffusion dynamics in aqueous 6M $NaClO_4$ solution. This clearly shows that the anisotropic FFCF will exhibit slower dynamics than the dynamics sampled with all laser polarizations parallel, the configuration used in the majority of hydroxyl stretch spectral diffusion studies. Independent of the anisotropy of the spectral diffusion, the anisotropic spectral memory does decay more quickly than the orientational memory, with only a small component of the FFCF persisting for multiple picoseconds. We believe this eliminates spectrally dependent rotational dynamics as a likely explanation for the large discrepancy between our results and those of Bakker and coworkers and leaves the origin of the discrepancy unresolved.

V. CLOSING REMARKS

We have presented a comprehensive theory for two species chemical exchange dynamics. This theory has extended prior developments[16,17] by instituting a thorough kinetic description of the orientational motions of the two interconverting species. We have successfully modeled the three dominant mechanisms for hydroxyl group rotation in water and aqueous solutions: the diffusive motion of the intact OH···O H-bond, the prompt large angular jumps associated with H-bond exchange, and a wobbling in a cone model for the librational motion of the water hydroxyl group about the OH···O H-bond. The kinetic model can be used in nonlinear response function calculations to model experimental nonlinear optical spectroscopy measurements with various polarization geometries, including polarization-selective pump-probe and 2DIR spectroscopy.

This model has been utilized to investigate the orientational dynamics in an aqueous solution of 6M $NaClO_4$ measured with polarization-selective two-dimensional IR spectroscopy and pump-probe measurements of the deuterated hydroxyl stretch in isotopically mixed water. The theoretical analysis of these measurements demonstrates that the large angular jump mechanism for H-bond exchange applies to hydroxyl groups switching between water–water H-bonds and water–perchlorate H-bonds. The theory and measurements also allow us to determine the orientational relaxation dynamics of the OD_W and OD_P H-bond configurations simultaneously from the polarization-selective pump-probe and 2DIR data. We observe the average orientational dynamics of both OD_W and OD_P configurations to proceed more slowly than isotopically mixed water, in support of our prior measurements.[36] Our findings exhibit qualitative agreement with the rotational correlation functions extracted from Car–Parinello molecular dynamics simulations of aqueous 6M $NaClO_4$ and water. We do not, however, reproduce the results of Bakker and co-workers, who observed the orientational dynamics of OD_W hydroxyl groups to be indistinguishable from isotopically mixed water.[43] The spectral bandwidth of the pump pulses represents the primary distinction between the two experimental approaches, indicating that a frequency dependent orientational relaxation rate could explain the discrepancy between the measurements, but the experimentally measured spectral diffusion dynamics of the OD_W configuration proceed too quickly for this explanation to be viable. Despite this discrepancy, our time resolved vibrational spectroscopy measurements, as well as those of Omta *et al.*, clearly indicate the power of vibrational anisotropy measurements for acquiring molecular scale information about the hydrogen bonding dynamics in aqueous systems.

ACKNOWLEDGMENTS

This research was supported through the PULSE Institute at the SLAC National Accelerator Laboratory by the U.S. Department of Energy, Office of Basic Energy Sciences. We would like to thank Sungnam Park and Michael Odelius for their important contributions to earlier stages of this research.

[1] K. Ando and J. T. Hynes, J. Mol. Liq. **64**, 25 (1995).
[2] T. C. Berkelbach, H. S. Lee, and M. E. Tuckerman, Phys. Rev. Lett. **103**, 4 (2009).
[3] P. Ball, Chem. Rev. **108**, 74 (2008).
[4] G. Stirnemann and D. Laage, J. Phys. Chem. Lett. **1**, 1511 (2010).
[5] D. E. Moilanen, E. E. Fenn, Y.-S. Lin, J. L. Skinner, B. Bagchi, and M. D. Fayer, Proc. Natl. Acad. Sci. U.S.A. **105**, 5295 (2008).
[6] D. Laage and J. T. Hynes, Science **311**, 832 (2006).
[7] D. Laage and J. T. Hynes, J. Phys. Chem. B **112**, 14230 (2008).
[8] D. Laage and J. T. Hynes, Proc. Natl. Acad. Sci. U.S.A. **104**, 11167 (2007).
[9] M. Ji, M. Odelius, and K. J. Gaffney, Science **328**, 1003 (2010).
[10] J. Zheng, K. Kwak, J. Asbury, X. Chen, I. R. Piletic, and M. D. Fayer, Science **309**, 1338 (2005).

[11]S. Woutersen, Y. Mu, G. Stock, and P. Hamm, Chem. Phys. **266**, 137 (2001).
[12]M. Ji, S. Park, and K. J. Gaffney, J. Phys. Chem. Lett. **1**, 1771 (2010).
[13]J. F. Cahoon, K. R. Sawyer, J. P. Schlegel, and C. B. Harris, Science **319**, 1820 (2008).
[14]S. Park, M. Ji, and K. J. Gaffney, J. Phys. Chem. B **114**, 6693 (2010).
[15]K. J. Tielrooij, N. Garcia-Araez, M. Bonn, and H. J. Bakker, Science **328**, 1006 (2010).
[16]K. Kwak, J. Zheng, H. Cang, and M. D. Fayer, J. Phys. Chem. B **110**, 19998 (2006).
[17]O. Golonzka and A. Tokmakoff, J. Chem. Phys. **115**, 297 (2001).
[18]M. Khalil, N. Demirdoven, and A. Tokmakoff, J. Phys. Chem. A **107**, 5258 (2003).
[19]D. W. G. Smith and J. G. Powles, Mol. Phys. **10**, 451 (1966).
[20]J. C. Hindman, A. Svirmickas, and M. Wood, J. Chem. Phys. **59**, 1517 (1973).
[21]T. Tao, Biopolymers **8**, 609 (1969).
[22]A. Szabo, J. Chem. Phys. **81**, 150 (1984).
[23]G. R. Fleming, *Chemical Applications of Ultrafast Spectroscopy* (Oxford, New York, 1986).
[24]M. Lim, T. A. Jackson, and P. A. Anfinrud, Nat. Struct. Mol. Biol. **4**, 209 (1997).
[25]A. B. Myers, R. M. Hochstrasser, IEEE J. Quantum Electron. **QE-22**, 1482 (1986).
[26]H. G. Purucker, V. Tunkin, and A. Laubereau R. Raman, Spectrosc. **24**, 453 (1993).
[27]C. Z. Wan and C. K. Johnson, J. Chem. Phys. **99**, 7602 (1993).
[28]A. Tokmakoff, J. Chem. Phys. **105**, 1 (1996).
[29]P. Debye, Physik. Z. **36**, 100 (1935).
[30]B. J. Berne and R. Pecora, *Dynamic Light Scattering: With Applications to Chemistry, Biology, and Physics* (R. E. Krieger Publishing Co., Malabar, FL, 1990).
[31]G. Lipari and A. Szabo, Biophys. J. **30**, 489 (1980).
[32]K. Kinosita, S. Kawato, and A. Ikegami, Biophys. J. **20**, 289 (1977).
[33]E. N. Ivanov, Sov. Phys. JETP **18**, 1041 (1964).
[34]K. Kwac, C. Lee, Y. Jung, J. Han, K. Kwak, J. R. Zheng, M. D. Fayer, and M. Cho, J. Chem. Phys. **125** (2006).
[35]O. Golonzka, M. Khalil, N. Demirdoven, and A. Tokmakoff, J. Chem. Phys. **115**, 10814 (2001).
[36]S. Park, M. Odelius, and K. J. Gaffney, J. Phys. Chem. B **113**, 7825 (2009).
[37]D. E. Moilanen, D. Wong, D. E. Rosenfeld, E. E. Fenn, and M. D. Fayer, Proc. Natl. Acad. Sci. U.S.A. **106**, 375 (2009).
[38]M. T. Zanni, N. H. Ge, Y. S. Kim, and R. M. Hochstrasser, Proc. Natl. Acad. Sci. U. S. A. **98**, 11265 (2001).
[39]E. L. Read, G. S. Engel, T. R. Calhoun, T. Mančal, T. K. Ahn, R. E. Blankenship, and G. R. Fleming, Proc. Natl. Acad. Sci. U.S.A. **104**, 14203 (2007).
[40]M. E. Rose, *Elementary Theory of Angular Momentum* (Dover, New York, 1957).
[41]See supplementary material at http://dx.doi.org/10.1063/1.3530783 for the cone integral method, full expression of the F^{ij} function and the 2D spectra used for CLS analysis, etc.
[42]Y. L. A. Rezus and H. J. Bakker, J. Chem. Phys. **123**, 114502 (2005).
[43]A. W. Omta, M. F. Kropman, S. Woutersen, and H. J. Bakker, Science **301**, 347 (2003).
[44]S. Park, D. E. Moilanen, and M. D. Fayer, J. Phys. Chem. B **112**, 5279 (2008).
[45]S. Mukamel, *Principles of Nonlinear Optical Spectroscopy* (Oxford University Press, New York, 1995).
[46]S. Park, K. Kwak, and M. D. Fayer, Laser Phys. Lett. **4**, 704 (2007).
[47]Y. Marcus, Chem. Rev. **109**, 1346 (2009).
[48]C. P. Lawrence, and J. L. Skinner, J. Chem. Phys. **118**, 264 (2003).
[49]J. B. Asbury, T. Steinel, C. Stromberg, S. A. Corcelli, C. P. Lawrence, J. L. Skinner, and M. D. Fayer, J. Phys. Chem. A **108**, 1107 (2004).
[50]K. B. Moller, R. Rey, and J. T. Hynes, J. Phys. Chem. A **108**, 1275 (2004).